

Phase control of localization in the nonlinear two-mode system from harmonic mixing driving: Perturbative analysis and symmetry consideration

Xianchao Le¹, Zhao-Yun Zeng², Baiyuan Yang², Yunrong Luo³, Jinpeng Xiao²,
Lei Li², Lisheng Wang², Yajiang Chen², Ai-Xi Chen¹, and Xiaobing Luo^{1,2*}

¹*Department of Physics, Zhejiang Sci-Tech University, Hangzhou, 310018, China*

²*School of Mathematics and Physics, Jinggangshan University, Ji'an 343009, China and*

³*Department of Physics and Key Laboratory for Matter Microstructure and Function of Hunan Province, and Key Laboratory of Low-dimensional Quantum Structures and Quantum Control of Ministry of Education, Hunan Normal University, Changsha 410081, China*

(Dated: July 12, 2022)

In this paper, we present a rigorous analysis of symmetry and underlying physics of the nonlinear two-mode system driven by a harmonic mixing field, by means of multiple scale asymptotic analysis method. The effective description in the framework of the second-order perturbative theory provides an accurate picture for understanding the Floquet eigenspectrum and dynamical features of the nonlinear two-mode system, showing full agreement with the prediction of symmetry considerations. We find that two types of symmetries play significant role in the dynamical features of this model, the mechanism behind which can be interpreted in terms of the effective description. The results are of relevance for the phase control of the atomic localization in Bose-Einstein condensates or switch of the optical signals in nonlinear mediums.

Keywords: Symmetry, Multiple time scales, Nonlinear Floquet states, Localization

I. INTRODUCTION

Nonlinear two-mode model is one prototypical example to investigate the fundamental quantum effects and nonlinear tunneling dynamics. The existence of nonlinearity is ubiquitous in diverse branches of science and its physical origins include a mean-field treatment of the interactions between coherent atoms[1], nonlinear Kerr effects in optical fibers[2], and possible modifications of quantum mechanics on the fundamental level[3]. In reality, the nonlinear two-mode model can be applied to describe a wide variety of physical systems, such as two coupled optical waveguides with Kerr nonlinearity[4], Bose-Einstein condensates (BECs) in a double-well potential[5], among others. As is well known, the presence of nonlinearity gives rise to a number of new quantum natures such as macroscopic quantum self-trapping (MQST)[5–7] and breakdown of quantum adiabaticity[8–10], which presents both challenges and opportunities for existing theories in linear systems.

In recent years, Floquet engineering, i.e., coherent control via periodic driving, has offered a versatile method for realization of new phases not accessible in equilibrium systems[11–14], because it adds time-periodicity as a novel control dimension to quantum systems. Nonlinear two-mode model under periodic driving presents the paradigm of this hot topic and thus is attracting more and more interest, due to the fact that gaining insight from the combined effects of periodic driving and nonlinearity on the quantum tunneling through a barrier may contribute to the possibility of utilizing two-state systems as the basic building blocks of quantum-based devices. In periodically driven quantum systems, it is convenient to analyze the dynamics in terms of the so-called Floquet

states and quasi-energies. When nonlinearity is introduced, it is necessary to extend the conventional Floquet states to nonlinear Floquet states[15–19]. Nowadays considerable efforts have been devoted to study the periodically driven nonlinear two-state systems in different ways, i.e., by employing an effective Hamiltonian description[20, 21], numerically computing the nonlinear Floquet quasienergy spectrum[17–19, 22, 23], and constructing the exact analytical nonlinear Floquet solutions[24–26] as well. Rich dynamical behaviors have been uncovered, such as the emergence of Hamiltonian chaos[27–31], photon-assisted tunneling[32, 33], coherent control of self-trapping[15, 16, 20, 24], and so on.

On the other side, previous works have clearly identified that the symmetries of the time-periodic Hamiltonian play crucial role in the current rectification phenomenon or the ratchet effect in the driven periodic potential[34, 35]. It has been shown that in order to achieve directed (ratchet) transport, relevant symmetries have to be broken[36, 37]. According to the Curie's principle, a certain phenomenon always occurs unless it is ruled out by symmetries[34]. The discussion of space-time symmetries was also exemplified nicely by the two-state dynamics[38]. It has been noted that a broken space-time symmetry leads in general to a driving-induced unbalanced Floquet states with unequal population of two modes. In addition, a prominent quantum effect called coherent destruction of tunneling (CDT)[39], upon the occurrence of which the quantum tunneling effects can be completely suppressed, has been shown to be connected to the degeneracy of the quasienergies and the so-called generalized parity symmetry (that is, the Hamiltonian is invariant under a spatial parity transformation plus a time shift by half a driving period)[38]. An important question now arises as to how the symmetry pictures are modified when the two-state system is subject to nonlinearity. Despite a few numerical studies available in such a problem, the connection between symmetry and dynamical properties of the driven nonlinear two-mode model is still not

*Corresponding author: xiaobingluo2013@aliyun.com

very clear, which awaits more rigorous and elaborate analytical results.

In the present work, we shall explore the symmetry and the underlying physics of the nonlinear two-state system exposed to a harmonic mixing field, in a rigorous way by means of multiple-scale asymptotic analysis method. By pushing the multiple-time-scale asymptotic analysis up to the second order, it is shown that apart from renormalization of the tunneling parameter, the harmonic mixing driving may also induce an effective static dc-bias between two modes whose amplitude and sign depend on the phase shift between two harmonics. The effective time-independent Hamiltonian obtained in the framework of the second-order perturbative theory is found to be successful in capturing the fine structure of the quasienergy spectrum with different time-space symmetries, which confirms the predictions of the symmetry considerations. The analytical results give a clear explanation for why the phase shift between the two-harmonics components of driving field can play the role of control parameter for the amplitude and sign of the population imbalance of nonlinear Floquet states.

II. MODEL AND SYMMETRY

We consider a simple, yet non-trivial periodically driven nonlinear two-mode system consisting of two basis states $|1\rangle$ and $|2\rangle$, whose dynamics is described by

$$\begin{aligned} i\frac{dc_1}{dt} &= -\frac{\nu}{2}c_2 + \frac{S(t)}{2}c_1 - \chi|c_1|^2c_1 \\ i\frac{dc_2}{dt} &= -\frac{\nu}{2}c_1 - \frac{S(t)}{2}c_2 - \chi|c_2|^2c_2, \end{aligned} \quad (1)$$

where ν denotes the tunneling rate constant, χ is the nonlinearity strength, $c_{1,2}$ are the quantum probability amplitudes on the two basis states $|1\rangle$ and $|2\rangle$, and $S(t)$ is an external periodic field of zero mean, $S(t+T) = S(t)$.

Before proceeding to the analysis of dynamics of the system (1), it is instructive to identify the symmetry property of the model equation. Like its linear counterpart, the driven nonlinear two-mode system also admits solutions in the form of Floquet states $\mathbf{c}(t) = \tilde{\mathbf{c}}(t)e^{-i\epsilon t}$, where $\mathbf{c}(t) = [c_1(t), c_2(t)]^T$ (hereafter the superscript T stands for the transpose), ϵ is the quasienergy, and $\tilde{\mathbf{c}}(t) = [\tilde{c}_1(t), \tilde{c}_2(t)]^T$ inherits the period of the driving and is called the Floquet eigenstate. Substituting the Floquet solution into Eq. (1), we obtain the following eigenvalue equation

$$\mathcal{H}\tilde{\mathbf{c}}(t) = \epsilon\tilde{\mathbf{c}}(t), \quad \mathcal{H} := H(t) - i\partial_t, \quad (2)$$

with time-periodic Hamiltonian corresponding to the system (1), i.e.,

$$H(t) = \begin{pmatrix} \frac{S(t)}{2} - \chi|\tilde{c}_1(t)|^2 & -\frac{\nu}{2} \\ -\frac{\nu}{2} & -\frac{S(t)}{2} - \chi|\tilde{c}_2(t)|^2 \end{pmatrix}, \quad (3)$$

where the operator \mathcal{H} is the so-called Floquet Hamiltonian defined in the extended Hilbert space.

For the linear ($\chi = 0$) case, we should review the three relevant symmetries of (2) below. If $S(t)$ is shift symmetric $S(t) = -S(t+T/2)$, then \mathcal{H} is invariant under the generalized parity symmetry

$$S_{\text{GP}} : |1\rangle \leftrightarrow |2\rangle, \quad t \rightarrow t + \frac{T}{2}, \quad (4)$$

which consists of a spatial parity transformation plus a time shift by half a driving period.

If $S(t)$ is antisymmetric under $t \rightarrow -t + 2t_0$ inversion, $S(t+t_0) = -S(-t+t_0)$ at some appropriate points t_0 , the Floquet Hamiltonian is invariant under the following symmetry

$$S_{\text{PT}} : |1\rangle \leftrightarrow |2\rangle, \quad t \rightarrow -t + 2t_0, i \rightarrow -i, \quad (5)$$

which is equivalent to parity-time symmetry. The transformation S_{PT} represents the combined parity and time reversal operations.

Furthermore, if $S(t)$ possesses the symmetry $S(t+t_0) = S(-t+t_0)$, then the Floquet Hamiltonian \mathcal{H} is time-reversal invariant under

$$S_{\text{T}} : t \rightarrow -t + 2t_0, i \rightarrow -i. \quad (6)$$

To measure the localization properties of a Floquet mode, we use the time-averaged expectation values of the Pauli matrix σ_z :

$$\langle\langle\sigma_z\rangle\rangle = \frac{1}{T} \int_0^T dt \tilde{\mathbf{c}}^\dagger(t) \sigma_z \tilde{\mathbf{c}}(t). \quad (7)$$

This time-averaged expectation value $\langle\langle\sigma_z\rangle\rangle$ would vanish with a perfectly delocalized Floquet state (balanced Floquet state).

In the linear limit ($\chi = 0$), it can be readily verified that the system (1) has two Floquet states with zero time-averaged population imbalances, namely $\langle\langle\sigma_z\rangle\rangle = 0$, whenever the symmetries S_{GP} and/or S_{PT} are realized.

Next we will show what consequences arise for the above mentioned symmetries when the nonlinearity is imposed. Consider a harmonic mixing (two-frequency) driving

$$S(t) = -A[\sin\omega t + f \sin(2\omega t + \phi)], \quad (8)$$

which has two components of frequencies ω and 2ω with phase shift ϕ . Obviously, in the presence of both harmonics ($A \neq 0, f \neq 0$), the generalized parity symmetry S_{GP} is always violated, independently of the value of the phase shift ϕ . Note that the antisymmetry $S(t) = -S(-t)$ is preserved for $\phi = n\pi$ with n integer, and the time-reversal symmetry $S(t_0+t) = S(t_0-t)$ is preserved for $\phi = n\pi + \pi/2$.

The relationship between the antisymmetry $S(t) = -S(-t)$ and dynamical properties can be readily analyzed by the symmetry argument. We implement S_{PT} on the nonlinear model Eq. (2), where S_{PT} includes the combined parity and time reversal operations. As the first step, time-reversal transformation (which changes a complex number to its complex conjugate and turns t into $-t$) convert Eq. (2) into

$$[\tilde{H} - i\partial_t] \begin{pmatrix} \tilde{c}_1^*(-t) \\ \tilde{c}_2^*(-t) \end{pmatrix} = \epsilon \begin{pmatrix} \tilde{c}_1^*(-t) \\ \tilde{c}_2^*(-t) \end{pmatrix}, \quad (9)$$

with

$$\tilde{H} = \begin{pmatrix} \frac{S(-t)}{2} - \chi|\tilde{c}_1^*(-t)|^2 & -\frac{\nu}{2} \\ -\frac{\nu}{2} & -\frac{S(-t)}{2} - \chi|\tilde{c}_2^*(-t)|^2 \end{pmatrix}. \quad (10)$$

The second step is to act with the parity transformation (permutation of the two indices 1 and 2) on Eq. (9), from which we can observe

$$\mathcal{H}' \begin{pmatrix} \tilde{c}_2^*(-t) \\ \tilde{c}_1^*(-t) \end{pmatrix} = \varepsilon \begin{pmatrix} \tilde{c}_2^*(-t) \\ \tilde{c}_1^*(-t) \end{pmatrix} \quad (11)$$

with

$$\mathcal{H}' = \begin{pmatrix} -\frac{S(-t)}{2} - \chi|\tilde{c}_2^*(-t)|^2 & -\frac{\nu}{2} \\ -\frac{\nu}{2} & \frac{S(-t)}{2} - \chi|\tilde{c}_1^*(-t)|^2 \end{pmatrix} - i\partial_t. \quad (12)$$

By comparing Eq. (12) with its original equation (2), we find that for a nonlinear system under the action of antisymmetric driving [$S(t) = -S(-t)$], the S_{PT} operation leaves the Floquet Hamiltonian invariant, namely $\mathcal{H}' = \mathcal{H}$, provided that the following constraint,

$$\chi|\tilde{c}_2(-t)| = \chi|\tilde{c}_1(t)|, \quad (13)$$

is satisfied. If the Floquet Hamiltonian is invariant under S_{PT} , we have

$$S_{PT} \begin{pmatrix} \tilde{c}_1(t) \\ \tilde{c}_2(t) \end{pmatrix} = \begin{pmatrix} \tilde{c}_2^*(-t) \\ \tilde{c}_1^*(-t) \end{pmatrix} = \begin{pmatrix} \tilde{c}_1(t) \\ \tilde{c}_2(t) \end{pmatrix} e^{i\varphi}. \quad (14)$$

Here the Floquet states are defined up to an arbitrary phase φ . Physically, Eq. (14) implies that the Floquet Hamiltonian operator \mathcal{H} and the S_{PT} operator share the same eigenmode. Once Eq. (14) is satisfied, the constraint (13) is satisfied automatically and vice versa.

From (14), it is easy to prove

$$\frac{1}{T} \int_0^T |\tilde{c}_2(t)|^2 dt = \frac{1}{T} \int_0^T |\tilde{c}_1(t)|^2 dt, \quad (15)$$

which means $\langle\langle\sigma_z\rangle\rangle = \frac{1}{T} \int_0^T [|c_1(t)|^2 - |c_2(t)|^2] dt = 0$, representing balanced Floquet states with zero averaged population imbalances. Apparently, whether nonlinearity presents or not, the balanced Floquet states exist inevitably for the antisymmetric driving. Nevertheless, if the antisymmetry $S(t) = -S(-t)$ is violated, the balanced Floquet states will disappear since the Floquet Hamiltonian changes under the action of operation S_{PT} , and all the Floquet states will acquire some nonzero population imbalances.

There are exceptions for the nonlinear case. If the antisymmetry $S(t) = -S(-t)$ holds, while $|\tilde{c}_1(t)|^2 = |\tilde{c}_2(-t)|^2$ does not hold, the Floquet Hamiltonian in (2) is not invariant under S_{PT} symmetry operation. This situation will lead to the surprising result that two doubly-degenerate unbalanced nonlinear Floquet states emerge, as described as follows. Due to $S(t) = -S(-t)$, from (2) and (12) it follows that the system admits two independent Floquet solutions $|\psi_1\rangle = [\tilde{c}_1(t), \tilde{c}_2(t)]^T$ and $|\psi_2\rangle = [\tilde{c}_2^*(-t), \tilde{c}_1^*(-t)]^T$ corresponding to the same quasienergy ε . In this case, because of $|\tilde{c}_1(t)|^2 \neq |\tilde{c}_2(-t)|^2$, it is easy to see that

$$\langle\langle\sigma_z\rangle\rangle = \frac{1}{T} \int_0^T [|c_1(t)|^2 - |c_2(t)|^2] dt \neq 0, \quad (16)$$

$$\frac{1}{T} \int_0^T \langle\psi_1|\sigma_z|\psi_1\rangle dt = -\frac{1}{T} \int_0^T \langle\psi_2|\sigma_z|\psi_2\rangle dt, \quad (17)$$

which denotes the emergence of two doubly-degenerate unbalanced (localized) nonlinear Floquet states, with exactly opposite time-averaged population imbalance. Apparently, these two degenerate Floquet states exist only when the nonlinear term does not vanish, so that they have no linear counterparts. Also note that the degeneracy for the nonlinear Floquet states can be lifted by breaking of the antisymmetry $S(t) = -S(-t)$.

III. QUASIENERGIES AND FLOQUET STATES

In this section, we shall numerically compute the nonlinear Floquet states and corresponding quasienergies by following the strategy developed in Refs. [17, 18]. In this strategy, we expand $\tilde{c}(t)$ as well as the time-periodic modulation $S(t)$ into Fourier series with $2N + 1$ modes: $\tilde{c}_1(t) = \sum_{n=-N}^N a_n e^{in\omega t}$, $\tilde{c}_2(t) = \sum_{n=-N}^N b_n e^{in\omega t}$, and $S(t) = \sum_{m=-N}^N p_m e^{im\omega t}$, $p_m = \frac{1}{T} \int_0^T S(t) e^{-im\omega t} dt$. Substituting these series into Eq. (2) yields

$$\begin{aligned} & \sum_{n,m} a_n p_m e^{i(m+n)\omega t} - \chi \sum_{n,m,m'} a_m a_{m'}^* a_n e^{i(m+n-m')\omega t} - \frac{\nu}{2} \sum_n b_n e^{in\omega t} \\ & + \sum_n n\omega a_n e^{in\omega t} = \varepsilon \sum_n a_n e^{in\omega t}, \\ & - \sum_{n,m} b_n p_m e^{i(m+n)\omega t} - \chi \sum_{n,m,m'} b_m b_{m'}^* b_n e^{i(m+n-m')\omega t} - \frac{\nu}{2} \sum_n a_n e^{in\omega t} \\ & + \sum_n n\omega b_n e^{in\omega t} = \varepsilon \sum_n b_n e^{in\omega t}. \end{aligned} \quad (18)$$

Multiplying the above equations by $e^{-ij\omega t}$, and integrating them over one driving period, one gets the following eigenvalue equation,

$$\begin{aligned} & -\frac{A}{4i} (a_{j-1} - a_{j+1} + f e^{i\phi} a_{j-2} - f e^{-i\phi} a_{j+2}) - \chi \sum_{m,m'} a_m a_{m'}^* a_{j+m'-m} \\ & - \frac{\nu}{2} b_j + j\omega a_j = \varepsilon a_j, \\ & \frac{A}{4i} (b_{j-1} - b_{j+1} + f e^{i\phi} b_{j-2} - f e^{-i\phi} b_{j+2}) - \chi \sum_{m,m'} b_m b_{m'}^* b_{j+m'-m} \\ & - \frac{\nu}{2} a_j + j\omega b_j = \varepsilon b_j. \end{aligned} \quad (19)$$

Finally, the nonlinear Floquet states and corresponding quasienergies can be found by solving numerically the eigenvalue equation (19) in a self-consistent manner. In numerical calculations, the Fourier terms of orders higher than a cut-off order N is neglected when convergence is achieved. The above procedure involves conservation of the norm, i.e.,

$$\sum_n |a_n|^2 + \sum_n |b_n|^2 = 1. \quad (20)$$

In analogy to quasimomenta in the spatially periodic crystal, the quasienergy spectrum repeats itself periodically on the energy-axis, thus possessing Brillouin zonelike structure, the

width of one zone being $\hbar\omega$ ($\hbar = 1$). In the following, we restrict ourselves to states with quasienergies in one Brillouin zone $(-\omega/2, \omega/2]$.

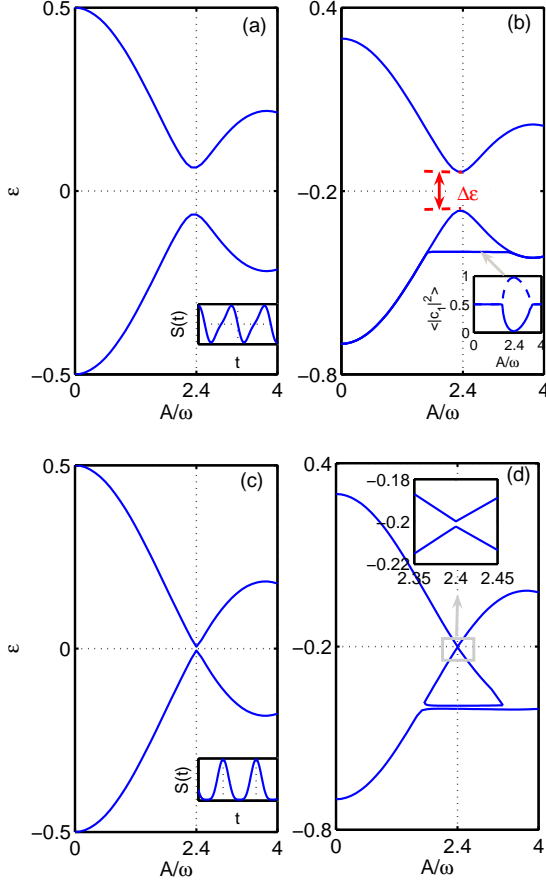


FIG. 1: (color online) The Floquet state quasienergies versus the driving parameter A/ω . [(a), (b)] the case of time-reversal antisymmetric driving [see the profile of $S(t)$ at $\phi = 0$, in the bottom-right inset of panel (a)]. [(c), (d)] the case of time-reversal symmetric driving [see the shape of $S(t)$ at $\phi = \pi/2$ in the inset of panel (c)]. The left column [(a), (c)] is for the linear case $\chi = 0$, while right column [(b), (d)] is for the nonlinear case $\chi = 0.4$. The inset of panel (b) shows the time-averaged population of mode 1 for every Floquet state in the lowest quasienergy level. Inset of panel (b) is the enlarged view of the closest approach of two normal Floquet states at $A/\omega = 2.4$. Other parameters: $f = 1/4$, $\omega = 10$, $v = 1$.

Our numerical results of quasienergies are plotted in Fig. 1. Figs. 1 (a)-(b) illustrate the quasienergies with an antisymmetric but a sawtooth driving [namely, $S(t) = -S(-t)$ with $\phi = 0$, see bottom-right inset in Fig. 1 (a)], and Figs. 1 (c)-(d) illustrate the ones with a symmetric driving [namely, $S(t + t_0) = S(-t + t_0)$ with $\phi = \pi/2$, see bottom-right inset in Fig. 1 (c)]. It is clear from Fig. 1 that there are two quasienergies at a given value of A/ω for the linear case (see the left column), while in the presence of nonlinearity several new states are emerging within certain range of A/ω due to bifurcation (see the right column). As the nonlinearity sets in, the antisymmetric driving case shows a pitchfork bifurcation

with appearance of the additional quasienergy level that is absent in the linear case and lies in the lowest branch. As seen in the inset of Fig. 1 (b), the additional quasienergy is in fact doubly degenerate and corresponds to two different Floquet states with exactly opposite nonzero population imbalance, which can be witnessed by calculation of the cycle-averaged population, $\langle |c_1|^2 \rangle = \frac{1}{T} \int_0^T |c_1|^2 dt$, for the given Floquet state. By contrast, for the symmetric driving [see Fig. 1 (d)], the twofold degeneracy for the lowest quasienergy is lifted and the quasienergy splits into two quasi-degenerate (nearly coincident) quasienergy levels. Among the two quasi-degenerate quasienergy levels that have no linear equivalent, the lower one shows strict continuation from the undriven limit, while the other emerges through the saddle-node bifurcation upon the smooth change of the driving parameter A/ω . It should be noted that there is no threshold value of nonlinearity for level bifurcation (forming the well-known triangular structure) to appear for the two-mode system under symmetric driving, which is the same as the purely sinusoidal driving case[17, 18]. However, for the antisymmetric driving case, our numerical results, which are not listed here, reveal that level bifurcation occurs only above a certain critical value of nonlinearity, the reason of which will be explained later. In addition to the new quasienergies emerging from bifurcation, there also exists two normal Floquet states which survive for vanishing nonlinearity and thus have linear counterparts. It is clear that the two normal Floquet states make closest approach at $A/\omega = 2.4$. A significant difference between the antisymmetric and symmetric case is that for the former, there exists a large gap between the two normal Floquet state levels [characterized by the minimal level spacing between the two Floquet states, see $\Delta\epsilon$ as labeled in Fig. 1 (b)], while for the latter, there is a nearly vanishing gap between the two normal levels when they make closest approach at $A/\omega = 2.4$. The enlarged view of the closest approach for the symmetric driving case reveals that there is no true level crossing between Floquet states.

In Fig. 2, we have numerically examined the dependence of the level spacing $\Delta\epsilon$ on the phase shift (top panel) and nonlinearity strength (bottom panel). As shown in Fig. 2 (a), for $\phi = \pm\pi/2$, i.e., in the presence a time-reversal symmetry, the energy gap $\Delta\epsilon$ nearly vanishes, and the maximum values of $\Delta\epsilon$ are reached for $\phi = n\pi$ with n integers (maximally broken time-reversal symmetry, but in the presence of a time-reversal antisymmetry). The dependence of $\Delta\epsilon$ on the nonlinearity strength is exemplified in Fig. 2 (a) for a specific case $\phi = \pi/4$. It is clearly seen that $\Delta\epsilon$ remains unchanged as the nonlinearity strength varies. The other choice of the phase shift will produce the same result. This means that the spectrum structures of the two normal Floquet states having linear counterparts are not affected by the presence of nonlinearity.

Most strikingly, switching the sign of phase shift ϕ creates the lowest Floquet states with opposite population imbalances, as shown in Fig. 3. By comparing Fig. 3 (a) and Fig. 3 (b), we clearly see that both cases of $\phi = \pm\pi/4$ have exactly the same quasienergy spectrum. For $\phi = \pm\pi/4$ (neither time-reversal symmetric nor time-reversal antisymmetric), there exists a level gap (no level crossing) between the

two normal Floquet states (see the two upper black lines) which have linear analogues, and when the nonlinearity is strong enough in this system [e.g., $\chi = 0.4$ in Fig. 3], there are two nearly coincident (not degenerate) quasienergy levels within a finite interval of parameter values around $A/\omega = 2.4$ (see the bottom insets), which stem from the level bifurcations caused by nonlinearity. In the insets of Fig. 3, we have also plotted the cycle-averaged population $\langle |c_1|^2 \rangle = \frac{1}{T} \int_0^T |c_1|^2 dt$ for the Floquet state corresponding to the lowest level. We may expect that the lowest Floquet state with nearly symmetric population distribution continuously evolves into the one with strong population imbalance. As A/ω is increased from zero to 2.4, we observe that the variable $\langle |c_1|^2 \rangle$ drops down to 0 for $\phi = -\pi/4$, which implies the complete localization at state $|2\rangle$, whereas $\langle |c_1|^2 \rangle$ rises up to 1 for $\phi = \pi/4$, corresponding to complete localization at state $|1\rangle$. Thus, by tuning the phase shift, we can switch between the two strongly localized states with opposite population imbalances.

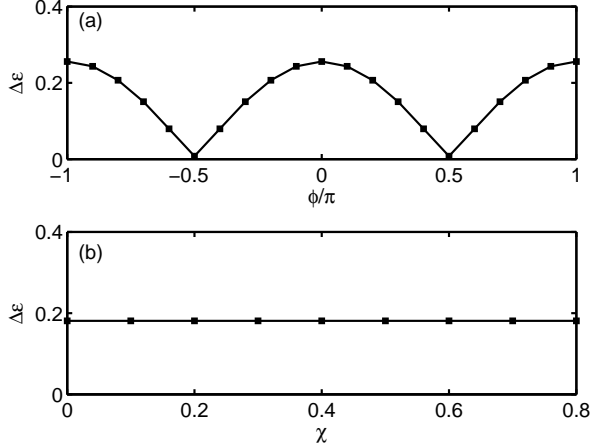


FIG. 2: (color online) (a) Dependence of $\Delta\epsilon$ on the phase shift ϕ . $f = 1/4$, $A/\omega = 2.4$, $\omega = 10$, $v = 1$, $\chi = 0.4$. (b) Dependence of $\Delta\epsilon$ on the nonlinearity parameter χ . $f = 1/4$, $\phi = \pi/4$, $A/\omega = 2.4$, $\omega = 10$, $v = 1$. The quantity $\Delta\epsilon$ denotes the minimal level spacing between the two normal Floquet states at $A/\omega = 2.4$, as indicated in Fig. 1 (b).

IV. PHYSICAL CONSEQUENCES

In this section, we will investigate the physical implications of the above-mentioned symmetries on the dynamics of nonlinear two-mode system. In Fig. 4, we initialize the system in state $|1\rangle$, and numerically plot the average of the population $|c_1|^2$ over long-enough time interval at $A/\omega = 2.4$ (a) and $A/\omega = 1$ (b) for $\phi = 0$ and $\phi = \pi/2$. By comparison, we find that at $A/\omega = 1$, the averages of the population $|c_1|^2$ for $\phi = 0$ and $\phi = \pi/2$ exhibit the same (overlapped) dynamics with the same transition to localization for nonlinearity strength above a critical value, while at $A/\omega = 2.4$, the averages show qualitatively different dynamical features for $\phi = 0$ and $\phi = \pi/2$. This can be explained by noting that the Floquet eigenspectra for $\phi = 0$ and $\phi = \pi/2$ are the same in the regions away

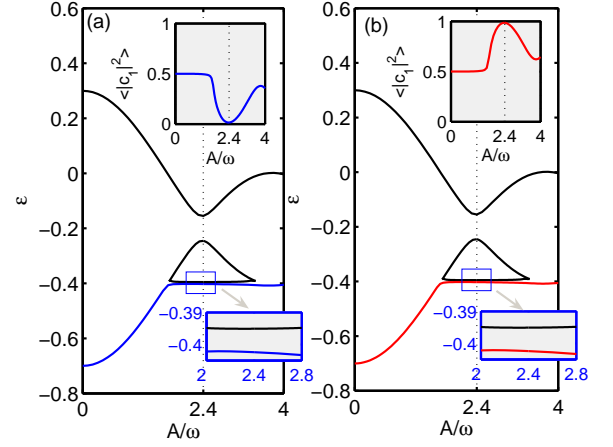


FIG. 3: (color online) The Floquet state quasienergies versus the driving parameter A/ω at (a) $\phi = -\pi/4$ and (b) $\phi = \pi/4$. In the two plots, the top-right insets are the time-averaged population $\langle |c_1|^2 \rangle$ for the Floquet state in the lowest quasienergy level, and the bottom-right insets are the enlarged view of the two quasi-degenerate (nearly coincident) quasienergy levels originating from nonlinear bifurcation. The other parameters are $f = 1/4$, $\omega = 10$, $v = 1$, $\chi = 0.4$.

from $A/\omega = 2.4$, but they are different in the region around $A/\omega = 2.4$. In Fig. 4 (a), for $\phi = \pi/2$ (time-reversal symmetric driving), we find that there is no threshold value of nonlinearity for localization to occur, which corresponds to an almost perfect (but not true) level crossing between the two normal Floquet states at $A/\omega = 2.4$. In this case, we notice the essential role played by the periodic driving on the localization phenomenon, and in the linear limit, this localization can be connected to the well-known CDT phenomenon. In contrast, if the time-reversal symmetry is broken [for example, $\phi = 0$ in Fig. 4 (a)], localization occurs only above a certain critical value of nonlinearity, suggesting the localization being a purely nonlinear phenomenon. This effect is related to the existence of a relatively large level gap ($\Delta\epsilon$) of the two normal Floquet states when they make closest approach at $A/\omega = 2.4$.

As noted in the previous section, the harmonic mixing driving field permits a sensitive control of the population distribution as a function of the phase shift. For demonstration, we simply ramp the driving amplitude A linearly in time, viz, $A = at$, where a is ramping rate. The system is initialized in its ground state, $c_1(0) = c_2(0) = 1/\sqrt{2}$. The driving amplitude is ramped up from zero to $A/\omega = 2.4$ for a given $\omega = 10$, then it is held constant hereafter. When the ramping rate takes a low value $a = 0.01$, we expect the system to adiabatically follow the lowest Floquet state. Two different scenarios of localization dynamics are identified in Fig. 5, for two different values of the phase shift ϕ . For $\phi = -\pi/4$, the time-evolving state is finally localized at $|2\rangle$ and stays there subsequently. When the phase shift is changed to a positive value, $\phi = \pi/4$, the time-evolving state becomes concentrated in the other basis state $|1\rangle$. Thus, states with opposite population imbalances can be selectively targeted, which may help to control localization process. To provide a more complete analysis on this phase control of population imbalance, we

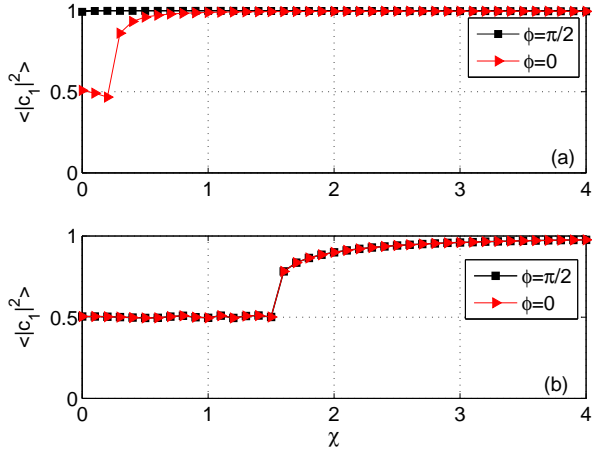


FIG. 4: (color online) Dependence of the time-averaged population $\langle |c_1|^2 \rangle$ on nonlinearity parameter χ at (a) $A/\omega = 2.4$ and (b) $A/\omega = 1$. Here the system is initially prepared at state $|1\rangle$, and the average $\langle \dots \rangle$ is numerically realized over a long-enough time interval. Two prototypical examples, namely $\phi = 0$ (not time-reversal symmetric but time-reversal antisymmetric) and $\phi = \pi/2$ (time-reversal symmetric) drivings, are compared. Other parameters are the same as in Fig. 1.

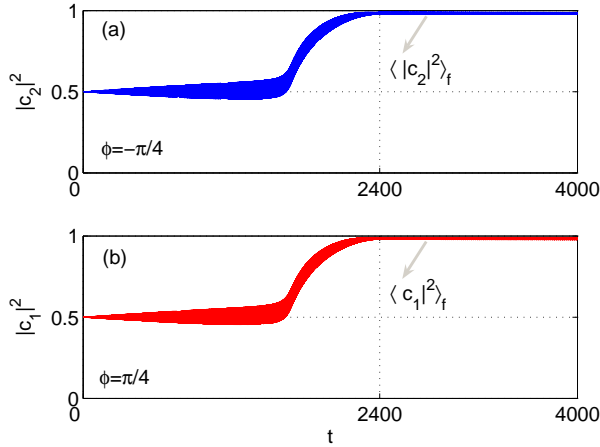


FIG. 5: (color online) Localization induced by the modulation $S(t)$ with a linearly ramped amplitude $A = \alpha t$, where the dimensionless ramping rate $\alpha = 0.01$, for the two-mode system (1) with two different values of ϕ . Ramping the modulation amplitude until $t = 2400$ (amounts to $A/\omega = 2.4$) gives the maximum localization at the basis state $|2\rangle$ (blue curve, $\phi = -\pi/4$), or the other basis state $|1\rangle$ (red curve, $\phi = \pi/4$). Holding A constant after the certain time ($t = 2400$, marked by the vertical line) keeps the localization at a constant level. The system is initialized in its ground state, $c_1(0) = c_2(0) = 1/\sqrt{2}$, and the other parameters are the same as in Fig. 3.

evaluate the final time-averaged population of the two modes as $\langle |c_n|^2 \rangle_f = \frac{1}{\Delta t} \int_{t_f}^{t_f + \Delta t} |c_n|^2 dt$, ($n = 1, 2$), where t_f represents the time instant when the linearly-ramping modulation amplitude reaches the value $A/\omega = 2.4$ (giving the maximum localization), and Δt represents the long-enough averaging time interval (during which the modulation amplitude stays constant). As expected, the degree of final localization is sym-

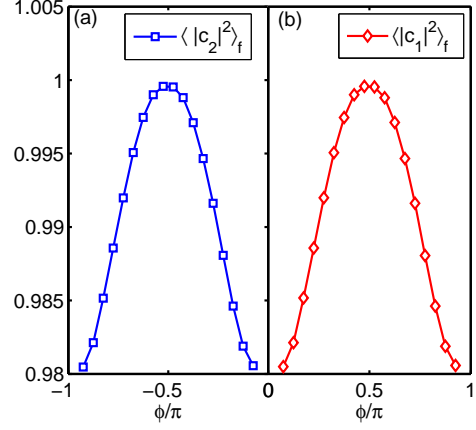


FIG. 6: (color online) The final localization according to the adiabatic process outlined in Fig. 5 as a function of phase shift ϕ . Here the localization is quantified by the final time-averaged population of the two modes as $\langle |c_n|^2 \rangle_f = \frac{1}{\Delta t} \int_{t_f}^{t_f + \Delta t} |c_n|^2 dt$, ($n = 1, 2$), where $t_f = 2400$ and the averaging time $\Delta t = 400$ are used. The initial condition and system parameters are the same as in Fig. 5.

metric with respect to $\phi = 0$ [see Fig. 6], and which one of the two basis states is highly occupied depends on the sign of the phase shift.

Now it is natural to put a simple question: why can the change of the phase shift lead to inversion of population imbalance? At present, the analytical results for the question is still missing in the literatures, and thus this problem calls for analytical insights.

V. PERTURBATIVE ANALYSIS

To gain analytical insight, in this section we perform a multiple-scale asymptotic analysis of the model (1) in the high frequency limit $\omega \gg \{v, \chi\}$ (see, for instance, Refs. [40–43]). For this purpose, we first introduce the slowly varying functions a_1 and a_2 through the transformation

$$c_1 = a_1 e^{-i \int \frac{S(t)}{2} dt}, \quad c_2 = a_2 e^{i \int \frac{S(t)}{2} dt}. \quad (21)$$

Substituting the transformation (21) into Eq. (1), we obtain the following coupled equation

$$\begin{aligned} i \frac{da_1}{dt} &= -\frac{v'}{2} a_2 - \chi |a_1|^2 a_1, \\ i \frac{da_2}{dt} &= -\frac{v'^*}{2} a_1 - \chi |a_2|^2 a_2, \end{aligned} \quad (22)$$

where $v' = v e^{i \int S(t) dt} = v \exp [i \frac{A}{\omega} \cos \omega t + i \frac{A f}{2\omega} \cos(2\omega t + \phi)]$.

Denoting

$$F(t) = \exp [i \frac{A}{\omega} \cos \omega t + i \frac{A f}{2\omega} \cos(2\omega t + \phi)], \quad (23)$$

and introducing a new variable

$$\tau = \omega t, \quad \epsilon = \frac{v}{\omega}, \quad (24)$$

then Eq. (22) reads as

$$\begin{aligned} i\frac{da_1}{d\tau} &= -\frac{\epsilon}{2}F(\tau)a_2 - \epsilon\frac{\chi}{v}|a_1|^2a_1, \\ i\frac{da_2}{d\tau} &= -\frac{\epsilon}{2}F^*(\tau)a_1 - \epsilon\frac{\chi}{v}|a_2|^2a_2. \end{aligned} \quad (25)$$

Let us look for a solution to Eq. (25) as a power-series expansion in the smallness parameter ϵ :

$$a_j = a_j^{(0)} + \epsilon a_j^{(1)} + \epsilon^2 a_j^{(2)} + \dots, \quad j = 1, 2, \quad (26)$$

and introduce multiple time scales $T_0 = \tau$, $T_1 = \epsilon\tau$, $T_2 = \epsilon^2\tau, \dots$

By using the derivative rule $\frac{d}{d\tau} = \frac{\partial}{\partial T_0} + \epsilon\frac{\partial}{\partial T_1} + \epsilon^2\frac{\partial}{\partial T_2} + \dots$, and the fact

$$|a_j|^2 a_j = |a_j^{(0)}|^2 a_j^{(0)} + \epsilon[2|a_j^{(0)}|^2 a_j^{(1)} + (a_j^{(0)})^2 a_j^{*(1)}] + \dots, \quad j = 1, 2,$$

and substituting Eq. (26) into Eq. (25), we obtain a hierarchy of equations for successive corrections to $a_{1,2}$ at the various orders in ϵ . At the leading order ϵ^0 , we find

$$i\partial_{T_0} a_j^{(0)} = 0, \quad a_j^{(0)} = A_j(T_1, T_2, \dots), \quad j = 1, 2, \quad (27)$$

where the amplitudes $A_{1,2}(T_1, T_2, \dots)$ are functions of the slow time variables T_1, T_2, \dots , but independent of the fast time variable T_0 . At order ϵ^1 one has

$$\begin{aligned} i\partial_{T_1} a_1^{(0)} + i\partial_{T_0} a_1^{(1)} &= -\frac{F(\tau)}{2}a_2^{(0)} - \frac{\chi}{v}|a_1^{(0)}|^2 a_1^{(0)} \\ i\partial_{T_1} a_2^{(0)} + i\partial_{T_0} a_2^{(1)} &= -\frac{F^*(\tau)}{2}a_1^{(0)} - \frac{\chi}{v}|a_2^{(0)}|^2 a_2^{(0)}. \end{aligned} \quad (28)$$

For the convenience of our discussion, we simplify equation (28) as

$$\begin{aligned} i\partial_{T_1} A_1 + i\partial_{T_0} a_1^{(1)} &= -\frac{F(\tau)}{2}A_2 - \frac{\chi}{v}|A_1|^2 A_1 \\ i\partial_{T_1} A_2 + i\partial_{T_0} a_2^{(1)} &= -\frac{F^*(\tau)}{2}A_1 - \frac{\chi}{v}|A_2|^2 A_2. \end{aligned} \quad (29)$$

To avoid the occurrence of secularly growing terms in the solutions $a_1^{(1)}$ and $a_2^{(1)}$, the solvability conditions

$$i\partial_{T_1} A_1 = -\frac{\overline{F(\tau)}}{2}A_2 - \frac{\chi}{v}|A_1|^2 A_1, \quad i\partial_{T_1} A_2 = -\frac{\overline{F^*(\tau)}}{2}A_1 - \frac{\chi}{v}|A_2|^2 A_2 \quad (30)$$

must be satisfied. Throughout our paper, the overline denotes the time average with respect to the fast time variable T_0 . $F(\tau)$ can be expanded by using of the first kind Bessel function $J_\alpha(x)$ with order α ,

$$F(\tau) = \sum_{m,n} J_n\left(\frac{A}{\omega}\right) J_m\left(\frac{Af}{2\omega}\right) i^{m+n} e^{i(2m+n)\tau} e^{im\phi},$$

which gives

$$\overline{F(\tau)} = \sum_m J_{-2m}\left(\frac{A}{\omega}\right) J_m\left(\frac{Af}{2\omega}\right) i^{-m} e^{im\phi}. \quad (31)$$

It follows from Eqs. (29), (30) and (31), that the amplitudes $a_{1,2}^{(1)}$ at order ϵ are given by

$$\begin{aligned} a_1^{(1)} &= -i \int \left(-\frac{F(\tau)}{2}A_2 + \frac{\overline{F(\tau)}}{2}A_2\right) d\tau = A_2 \Phi(\tau), \\ a_2^{(1)} &= -i \int \left(-\frac{F^*(\tau)}{2}A_1 + \frac{\overline{F^*(\tau)}}{2}A_1\right) d\tau = -A_1 \Phi^*(\tau), \end{aligned} \quad (32)$$

where $\Phi(\tau) = \sum_{n \neq -2m} \frac{1}{2m+n} J_n\left(\frac{A}{\omega}\right) J_m\left(\frac{Af}{2\omega}\right) i^{m+n} e^{im\phi} e^{i(2m+n)\tau}$.

At the next order ϵ^2 , we have

$$\begin{aligned} i\left(\partial_{T_2} a_1^{(0)} + \partial_{T_1} a_1^{(1)} + \partial_{T_0} a_1^{(2)}\right) &= -\frac{F(\tau)}{2}a_2^{(1)} - \frac{\chi}{v}[2|a_1^{(0)}|^2 a_1^{(1)} \\ &\quad + (a_1^{(0)})^2 a_1^{*(1)}], \\ i\left(\partial_{T_2} a_2^{(0)} + \partial_{T_1} a_2^{(1)} + \partial_{T_0} a_2^{(2)}\right) &= -\frac{F^*(\tau)}{2}a_1^{(1)} - \frac{\chi}{v}[2|a_2^{(0)}|^2 a_2^{(1)} \\ &\quad + (a_2^{(0)})^2 a_2^{*(1)}]. \end{aligned} \quad (33)$$

In order to avoid the occurrence of secularly growing terms in the solutions $a_1^{(2)}$ and $a_2^{(2)}$, the following solvability conditions must be satisfied:

$$\begin{aligned} i\partial_{T_2} A_1 &= -\frac{\overline{F(\tau)}}{2}a_2^{(1)} = A_1 \frac{\overline{F(\tau)\Phi^*(\tau)}}{2} = \frac{\delta}{2}A_1, \\ i\partial_{T_2} A_2 &= -\frac{\overline{F(\tau)}}{2}a_1^{(1)} = -A_2 \frac{\overline{F^*(\tau)\Phi(\tau)}}{2} = -\frac{\delta^*}{2}A_2, \end{aligned} \quad (34)$$

where

$$\begin{aligned} \delta &= \overline{F(\tau)\Phi^*(\tau)} = \sum_{m,M,l,M \neq 0} \frac{(-1)^{M-l}}{M} i^{2M-m-l} e^{i(m-l)\phi} J_{M-2m}\left(\frac{A}{\omega}\right) \\ &\quad \times J_{M-2l}\left(\frac{A}{\omega}\right) J_m\left(\frac{Af}{2\omega}\right) J_l\left(\frac{Af}{2\omega}\right). \end{aligned} \quad (35)$$

Thus the evolution of the amplitudes $A_{1,2}$ up to the second-order long time scale is given by

$$i\frac{dA_j}{d\tau} = i\epsilon\partial_{T_1} A_j + i\epsilon^2\partial_{T_2} A_j, \quad j = 1, 2. \quad (36)$$

Substituting equations (27), (30) and (34) into equation (36), we obtain

$$\begin{aligned} i\frac{dA_1}{d\tau} &= -\epsilon\frac{\overline{F(\tau)}}{2}A_2 - \epsilon\frac{\chi}{v}|A_1|^2 A_1 + \epsilon^2\frac{\delta}{2}A_1, \\ i\frac{dA_2}{d\tau} &= -\epsilon\frac{\overline{F^*(\tau)}}{2}A_1 - \epsilon\frac{\chi}{v}|A_2|^2 A_2 - \epsilon^2\frac{\delta^*}{2}A_2. \end{aligned} \quad (37)$$

Substituting (24) into (37), we have

$$\begin{aligned} i\frac{dA_1}{dt} &= -v\frac{\overline{F(\tau)}}{2}A_2 - \chi|A_1|^2 A_1 + \frac{v^2}{\omega}\frac{\delta}{2}A_1, \\ i\frac{dA_2}{dt} &= -v\frac{\overline{F^*(\tau)}}{2}A_1 - \chi|A_2|^2 A_2 - \frac{v^2}{\omega}\frac{\delta^*}{2}A_2. \end{aligned} \quad (38)$$

Let $v' = v\overline{F(\tau)}$ and $\delta' = \frac{v^2}{\omega}\delta$, then Eq. (38) reads

$$i\frac{dA_1}{dt} = \frac{\delta'}{2}A_1 - \chi|A_1|^2 A_1 - \frac{v'}{2}A_2,$$

$$i\frac{dA_2}{dt} = -\frac{\delta'^*}{2}A_2 - \chi|A_2|^2A_2 - \frac{\nu'^*}{2}A_1. \quad (39)$$

Numerical investigations (not shown here) reveal that from Eq. (39) (which is accurate up to the time scale $\sim 1/\epsilon^2$), we can recover all the known quasienergy spectrums based on the original model (1). Thus, the effective equation (39) constitutes a strong analytical basis for understanding the dynamical features of the original system with different time-space symmetries. It is noteworthy that, in the effective equation (39), a second-order static dc-bias δ' appears as a surprise, apart from the coupling strength ν replaced by ν' . In the following, we will rigorously prove that the effective tunneling rate ν' and the second-order detuning δ' enjoy some very interesting properties.

(i) ν' is a real number when $\phi = \pm\pi/2$ [$\phi \in [-\pi, \pi]$], and is a complex number otherwise.

We write down

$$\overline{F(\tau)} = \sum_m J_{-2m}\left(\frac{A}{\omega}\right) J_m\left(\frac{Af}{2\omega}\right) i^{-m} e^{im\phi}, \quad (40)$$

and its complex conjugation

$$\overline{F(\tau)}^* = \sum_m J_{-2m}\left(\frac{A}{\omega}\right) J_m\left(\frac{Af}{2\omega}\right) (-i)^{-m} e^{-im\phi}. \quad (41)$$

Subtracting (41) from (40) yields

$$\begin{aligned} \overline{F(\tau)} - \overline{F(\tau)}^* &= \sum_m J_{-2m}\left(\frac{A}{\omega}\right) J_m\left(\frac{Af}{2\omega}\right) [e^{im(\phi - \frac{\pi}{2})} - e^{-im(\phi - \frac{\pi}{2})}] \\ &= 2i \sum_m J_{-2m}\left(\frac{A}{\omega}\right) J_m\left(\frac{Af}{2\omega}\right) \sin[m(\phi - \frac{\pi}{2})]. \end{aligned} \quad (42)$$

Evidently, when $\phi = \pm\pi/2$ [$\phi \in [-\pi, \pi]$], $\overline{F(\tau)} = \overline{F(\tau)}^*$, thus $\nu' = \nu\overline{F(\tau)}$ is a real number. If otherwise, i.e., when $\phi \neq \pm\pi/2$ [$\phi \in [-\pi, \pi]$], $\overline{F(\tau)}$ and $\nu' = \nu\overline{F(\tau)}$ are, in general, complex numbers.

(ii) δ' is always a real number.

By using the expression (35) of δ , one can obtain that

$$\begin{aligned} \delta^* &= \sum_{m,l,M,M \neq 0} \frac{(-1)^{M-l}}{M} (-i)^{2M-m-l} e^{-i(m-l)\phi} J_{M-2m}\left(\frac{A}{\omega}\right) J_{M-2l}\left(\frac{A}{\omega}\right) \\ &\quad \times J_m\left(\frac{Af}{2\omega}\right) J_l\left(\frac{Af}{2\omega}\right) \\ &= \sum_{m,l,M,M \neq 0} \frac{(-1)^{M-m}}{M} (-i)^{2M-m-l} e^{-i(l-m)\phi} J_{M-2m}\left(\frac{A}{\omega}\right) J_{M-2l}\left(\frac{A}{\omega}\right) \\ &\quad \times J_m\left(\frac{Af}{2\omega}\right) J_l\left(\frac{Af}{2\omega}\right). \end{aligned} \quad (43)$$

Here we have made the exchange $m \leftrightarrow l$. Since $(-1)^{M-m}(-1)^{2M-m-l} = (-1)^{M-l}$, we get from Eq. (43) that $\delta = \delta^*$, thus δ is a real number.

(iii) $\delta(-\phi) = -\delta(\phi)$, and δ must be zero when $\phi = 0$ [i.e., when $S(t)$ possesses the antisymmetry $S(t) = -S(-t)$].

Separating $M > 0$ and $M < 0$ parts of the expression (35) of δ , making the transformation $M \rightarrow -M$ for negative M , we

obtain

$$\begin{aligned} \delta &= \sum_{m,M,l,M>0} \frac{(-1)^{M-l}}{M} i^{2M-m-l} e^{i(m-l)\phi} J_{M-2m}\left(\frac{A}{\omega}\right) J_{M-2l}\left(\frac{A}{\omega}\right) \\ &\quad \times J_m\left(\frac{Af}{2\omega}\right) J_l\left(\frac{Af}{2\omega}\right) \\ &- \sum_{m,M,l,M>0} \frac{(-1)^{-M-l}}{M} i^{-2M-m-l} e^{i(m-l)\phi} J_{-M-2m}\left(\frac{A}{\omega}\right) \\ &\quad \times J_{-M-2l}\left(\frac{A}{\omega}\right) J_m\left(\frac{Af}{2\omega}\right) J_l\left(\frac{Af}{2\omega}\right). \end{aligned} \quad (44)$$

Changing the summation indices m, l into $-m, -l$ in the second summation in (44), we have

$$\begin{aligned} \delta &= \sum_{m,M,l,M>0} \frac{(-1)^{M-l}}{M} i^{2M-m-l} e^{i(m-l)\phi} J_{M-2m}\left(\frac{A}{\omega}\right) J_{M-2l}\left(\frac{A}{\omega}\right) \\ &\quad \times J_m\left(\frac{Af}{2\omega}\right) J_l\left(\frac{Af}{2\omega}\right) \\ &- \sum_{m,M,l,M>0} \frac{(-1)^{-M+l}}{M} i^{-2M+m+l} e^{-i(m-l)\phi} J_{-M+2m}\left(\frac{A}{\omega}\right) \\ &\quad \times J_{-M+2l}\left(\frac{A}{\omega}\right) J_m\left(\frac{Af}{2\omega}\right) J_l\left(\frac{Af}{2\omega}\right). \end{aligned} \quad (45)$$

By using the relation of Bessel function $J_{-\alpha} = (-1)^\alpha J_\alpha$ and the fact that $(-1)^{-m-l} = i^{-2m-2l}$, then we obtain the alternative form of δ from Eq. (45)

$$\begin{aligned} \delta &= \sum_{m,M,l,M>0} \frac{(-1)^{M-l}}{M} i^{2M-m-l} (e^{i(m-l)\phi} - e^{-i(m-l)\phi}) J_{M-2m}\left(\frac{A}{\omega}\right) \\ &\quad \times J_{M-2l}\left(\frac{A}{\omega}\right) J_m\left(\frac{Af}{2\omega}\right) J_l\left(\frac{Af}{2\omega}\right). \end{aligned} \quad (46)$$

When $\phi = 0$, it follows from Eq. (46) that $\delta = 0$. It is easy to see that $\delta(-\phi) = -\delta(\phi)$ from Eq. (46).

To corroborate these analytical results, we numerically calculate the two quantities $\overline{F(\tau)}$ and δ as shown in Fig. 7. The dependencies of $\overline{F(\tau)}$ on the driving parameter A/ω are illustrated in Figs. 7 (a) and (b) for $\phi = 0$ and $\phi = \pi/2$ respectively, which verifies the fact that $\overline{F(\tau)}$ [hence the effective coupling strength $\nu' = \nu\overline{F(\tau)}$] is a real number when $\phi = \pi/2$, and is generally a complex number when $\phi = 0$. Note that, if the time-reversal symmetry ($\phi = \pi/2$) is preserved, $\overline{F(\tau)}$ (consequently, the effective coupling strength) vanishes identically at some certain driving parameter values $A/\omega = 2.4, 5.4, 8.4$. Whereas if the time-reversal symmetry is violated [see, e.g., $\phi = 0$ in Fig. 7(a)], $\overline{F(\tau)}$ is not equal to zero for any value of A/ω . As shown in Fig. 7 (c), we also obtain a dependence of the effective detuning δ on ϕ with sign changes, as expected. We clearly observe that the effective detuning δ takes maximum (minimum) values at $\phi = \pm\pi/2$ (harmonic mixing signal is symmetric but not antisymmetric), but instead vanishes at $\phi = 0$ (harmonic mixing signal is antisymmetric).

The properties for $\overline{F(\tau)}$ and δ have the following physical implications. First, when $\phi = \pi/2$ such that the temporal symmetry $S(t + t_0) = S(-t + t_0)$ is preserved, $\overline{F(\tau)}$ vanishes at

$A/\omega = 2.4$, while δ takes nonzero value. The eigenvalues of Eq. (39) with an effectively undriven (time-averaged) Hamiltonian are the quasienergies of the original time-dependent quantum system (1). In the linear limit, from (39) we obtain the eigenvalues as $E_{\pm} = \pm \frac{1}{2} \sqrt{\delta'^2 + |\nu \overline{F(\tau)}|^2}$. When the driving parameter is chosen as $A/\omega = 2.4$ such that $\overline{F(\tau)}$ vanishes, there will be a minimum of the level spacing, which is fixed by an extremely small value $\Delta\varepsilon = \delta'$, and confirms that the quasienergies of the two normal Floquet states (having linear counterparts) form an anticrossing rather than a crossing. Thus, the common explanation of CDT fails. Here, the CDT for a time-reversal symmetric system comes from vanishing of the effective coupling strength, not from the quasienergy degeneracy. Second, when $\phi \neq \pi/2$ such that the time-reversal symmetry $S(t + t_0) = S(-t + t_0)$ is broken, $\overline{F(\tau)}$ (hence the effective coupling strength) does not vanish for any value of A/ω . As illustrated in Fig. 2 (b), the energy gap $\Delta\varepsilon$ (the minimum level spacing between two normal Floquet states) shows roughly no dependence on nonlinearity, and its value can be approximated (or accurately given) by $\Delta\varepsilon = \sqrt{\delta'^2 + |\nu \overline{F(\tau)}|^2}$ at $A/\omega = 2.4$, where $|\overline{F(\tau)}|$ takes minimum (nonzero) value. This approximation is made in the case $\delta' \neq 0$ (making the two normal Floquet states a little bit unbalanced), where we neglect the negligibly small nonlinear energy offset, i.e., the term $\chi(|A_1|^2 - |A_2|^2)$. Note that here the minimum value of $|\overline{F(\tau)}|$ is nonzero and much larger than the absolute value of second-order bias $|\delta'|$. Thus, the broken time-reversal symmetry leads to a relatively large energy gap $\Delta\varepsilon$ between the two normal Floquet states having linear counterparts. In this case, level bifurcation (resulting in the emergence of new localized nonlinear Floquet states) and suppression of tunneling occur only for nonlinearity beyond a certain threshold value. Third, the change of the phase shift can create the lowest Floquet states with opposite population imbalances. This can be reasoned as follows. When $\phi \neq 0$ [$S(t) \neq -S(-t)$], a nonzero second-order bias $\delta' = \frac{\nu^2}{\omega} \delta$ is generated by the broken time-reversal antisymmetry. When $\delta' \neq 0$, under inversion $\delta' \rightarrow -\delta'$, we conclude that for any eigenstate $(A'_1, A'_2)^T$ to (39), there is a partner eigenstate $(A'_2, A'_1)^T$ of (39) with δ' replaced by $-\delta'$ at the same energy. This implies inversion $\delta' \rightarrow -\delta'$ does not change the energy spectrum, but flip the sign of population imbalance corresponding to the same energy. Because of $\delta(-\phi) = -\delta(\phi)$, the inversion of population imbalance can be expected by changing the phase shift ϕ .

VI. CONCLUSION

In summary, the symmetry and underlying physics of the nonlinear two-state system driven by a harmonic mixing field have been studied analytically and numerically. A multiple-

scale asymptotic analysis is used to understand the essential physics with different time-space symmetries. By use of the effective description valid up to the second order of $1/\omega$, we have clarified the origin of the CDT in the time-reversal symmetric two-state system, and explained the reason why the

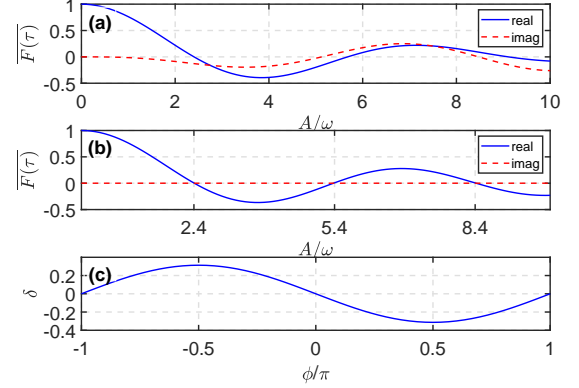


FIG. 7: (color online) $\overline{F(\tau)}$ (the renormalized factor of coupling strength) as a function of driving parameter A/ω for (a) $\phi = 0$ (breaking the temporal symmetry) and (b) $\phi = \pi/2$ (symmetric driving). The blue solid line and red dashed line denote the real and imaginary parts of $\overline{F(\tau)}$ respectively. (c) δ (describing the effective bias) as a function of phase shift ϕ at a particular driving parameter $A/\omega = 2.4$. The other parameters are $f = 1/4$, $\omega = 10$, $\nu = 1$, $\chi = 0.4$.

broken time-reversal antisymmetry can induce the inversion of population imbalance between two modes. These analytical results establish an intimate connection between symmetry breakings and the relevance of dynamical properties in the nonlinear two-mode system. Although various aspects of the nonlinear two-mode system have been explored previously, the analytical results on connection between symmetry and dynamical features of the system have not been addressed before and the present paper fills the gap in literatures.

Acknowledgments

The work was supported by the Natural Science Foundation of Zhejiang Province, China (Grant No. LY21A050002), the National Natural Science Foundation of China (Grant No. 11975110), the Scientific and Technological Research Fund of Jiangxi Provincial Education Department (Grant No. GJJ211026), and Zhejiang Sci-Tech University Scientific Research Start-up Fund (Grant No. 20062318-Y), the Scientific Research Foundation of Hunan Provincial Education Department (Grant No. 21B0063), and the Hunan Provincial Natural Science Foundation of China (Grant No. 2021JJ30435).

Xianchao Le and Zhao-Yun Zeng contributed equally.

- Diego: Academic, 2001
- [3] S. Weinberg, Precision tests of quantum mechanics, *Phys. Rev. Lett.* 62(5), 485 (1989)
 - [4] S. M. Jensen, The nonlinear coherent coupler, *IEEE J. Quantum Electron.* 18(10), 1580 (1982)
 - [5] A. Smerzi, S. Fantoni, S. Giovanzzi, and S. R. Shenoy, Quantum coherent atomic tunneling between two trapped Bose-Einstein condensates, *Phys. Rev. Lett.* 79(25), 4950 (1997)
 - [6] G. J. Milburn, J. Corney, E. M. Wright, and D. F. Walls, Quantum dynamics of an atomic Bose-Einstein condensate in a double-well potential, *Phys. Rev. A* 55(6), 4318 (1997)
 - [7] M. Albiez, R. Gati, J. Fölling, S. Hunsmann, M. Cristiani, and M. K. Oberthaler, Direct observation of tunneling and nonlinear self-trapping in a single bosonic Josephson junction, *Phys. Rev. Lett.* 95(1), 010402 (2005)
 - [8] B. Wu and Q. Niu, Nonlinear Landau-Zener tunneling, *Phys. Rev. A* 61(2), 023402 (2000)
 - [9] J. Liu, L. B. Fu, B. Y. Ou, S. G. Chen, D. I. Choi, B. Wu, and Q. Niu, Theory of nonlinear Landau-Zener tunneling, *Phys. Rev. A* 66(2), 023404 (2002)
 - [10] J. Liu, B. Wu, and Q. Niu, Nonlinear evolution of quantum states in the adiabatic regime, *Phys. Rev. Lett.* 90(17), 170404 (2003)
 - [11] M. Bukov, L. D'Alessio, and A. Polkovnikov, Universal high-frequency behavior of periodically driven systems: from dynamical stabilization to Floquet engineering, *Adv. Phys.* 64(2), 139 (2015)
 - [12] A. Eckardt, Colloquium: Atomic quantum gases in periodically driven optical lattices, *Rev. Mod. Phys.* 89(1), 011004 (2017)
 - [13] M. P. Silveri, J. A. Tuorila, E. V. Thuneberg, and G. S. Paraoanu, Quantum systems under frequency modulation, *Rep. Prog. Phys.* 80(5), 056002 (2017)
 - [14] S. Y. Bai, C. Chen, H. Wu, and J. H. An, Quantum control in open and periodically driven systems, *Advances in Physics: X* 6(1), 1870559 (2021)
 - [15] M. Holthaus, Towards coherent control of a Bose-Einstein condensate in a double well, *Phys. Rev. A* 64(1), 011601 (2001)
 - [16] M. Holthaus and S. Stenholm, Coherent control of the self-trapping transition, *Eur. Phys. J. B* 20(3), 451 (2001)
 - [17] X. B. Luo, Q. T. Xie, and B. Wu, Nonlinear coherent destruction of tunneling, *Phys. Rev. A* 76(5), 051802 (2007)
 - [18] X. B. Luo, Q. T. Xie, and B. Wu, Quasienergies and Floquet states of two weakly coupled Bose-Einstein condensates under periodic driving, *Phys. Rev. A* 77(5), 053601 (2008)
 - [19] L. Morales-Molina and S. Flach, Resonant ratcheting of a Bose-Einstein condensate, *New J. Phys.* 10(1), 013008 (2008)
 - [20] G. F. Wang, L. B. Fu, and J. Liu, Periodic modulation effect on self-trapping of two weakly coupled Bose-Einstein condensates, *Phys. Rev. A* 73(1), 013619 (2006)
 - [21] Q. Zhang, P. Hänggi, and J. B. Gong, Two-mode Bose-Einstein condensate in a high-frequency driving field that directly couples the two modes, *Phys. Rev. A* 77(5), 053607 (2008)
 - [22] L. Morales-Molina and J. B. Gong, Controlling the population imbalance of a Bose-Einstein condensate by a symmetry-breaking driving field, *Phys. Rev. A* 78, 041403 (2008)
 - [23] G. Lyu, L. K. Lim, and G. Watanabe, Floquet eigenspectra of a nonlinear two-mode system under periodic driving: The emergence of ring structures, *Phys. Rev. A* 101(5), 053623 (2020)
 - [24] Q. T. Xie, and W. H. Hai, Coherent control of self-trapping of two weakly coupled Bose-Einstein condensates, *Phys. Rev. A* 75(1), 015603 (2007)
 - [25] Q. T. Xie, Nonlinear Floquet solutions of two periodically driven Bose-Einstein condensates, *Phys. Rev. A* 76(4), 043622 (2007)
 - [26] B. Y. Yang, X. B. Luo, Q. L. Hu, and X. G. Yu, Exact control of parity-time symmetry in periodically modulated nonlinear optical couplers, *Phys. Rev. A* 94(4), 043828 (2016)
 - [27] F. Kh. Abdullaev and R. A. Kraenkel, Coherent atomic oscillations and resonances between coupled Bose-Einstein condensates with time-dependent trapping potential, *Phys. Rev. A* 62(2), 023613 (2000)
 - [28] C. H. Lee, W. H. Hai, L. Shi, X. W. Zhu, and K. L. Gao, Chaotic and frequency-locked atomic population oscillations between two coupled Bose-Einstein condensates, *Phys. Rev. A* 64(5), 053604 (2001)
 - [29] W. H. Hai, C. H. Lee, G. S. Chong, and L. Shi, Chaotic probability density in two periodically driven and weakly coupled Bose-Einstein condensates, *Phys. Rev. E* 66(2), 026202 (2002)
 - [30] C. Weiss and N. Teichmann, Differences between mean-field dynamics and N-particle quantum dynamics as a signature of entanglement, *Phys. Rev. Lett.* 100(14), 140408 (2008)
 - [31] H. Jiang, H. Susanto, T. M. Benson, and K. A. Cliffe, Equilibrium states and chaos in an oscillating double-well potential, *Phys. Rev. A* 89(1), 013828 (2014)
 - [32] A. Eckardt, T. Jinasundera, C. Weiss, and M. Holthaus, Analog of photon-assisted tunneling in a Bose-Einstein condensate, *Phys. Rev. Lett.* 95(20), 200401 (2005)
 - [33] G. Watanabe, Efficient creation of maximally entangled states by modulation of tunneling rates, *Phys. Rev. A* 81(2), 021604 (2010)
 - [34] P. Reimann, Brownian motors: noisy transport far from equilibrium, *Phys. Rep.* 361(2), 57 (2002)
 - [35] P. Hänggi and F. Marchesoni, Artificial Brownian motors: Controlling transport on the nanoscale, *Rev. Mod. Phys.* 81(1), 387 (2009)
 - [36] S. Flach, O. Yevtushenko, and Y. Zolotaryuk, Directed current due to broken time-space symmetry, *Phys. Rev. Lett.* 84(11), 2358 (2000)
 - [37] S. Denisov, L. Morales-Molina, S. Flach, and P. Hänggi, Periodically driven quantum ratchets: Symmetries and resonances, *Phys. Rev. A* 75(6), 063424 (2007)
 - [38] E. Kierig, U. Schnorrberger, A. Schietinger, J. Tomkovic, and M. K. Oberthaler, Single-particle tunneling in strongly driven double-well potentials, *Phys. Rev. Lett.* 100(19), 190405 (2008)
 - [39] F. Grossmann, T. Dittrich, P. Jung, and P. Hänggi, Coherent destruction of tunneling, *Phys. Rev. Lett.* 67(4), 516 (1991); Tunneling in a periodically driven bistable system, *Z. Phys. B* 84(2), 315 (1991)
 - [40] S. Longhi and G. Della Valle, Coherent destruction of tunneling of two interacting bosons in a tight-binding lattice, *Phys. Rev. A* 86(4), 042104 (2012)
 - [41] Z. Zhou, W. H. Hai, Q. T. Xie, and J. T. Tan, Second-order tunneling of two interacting bosons in a driven triple well, *New J. Phys.* 15(12), 123020 (2013)
 - [42] X. B. Luo, D. L. Wu, S. P. Luo, Y. Guo, X. G. Yu, and Q. L. Hu, Pseudo-parity-time symmetry in periodically high-frequency driven systems: perturbative analysis, *J. Phys. A* 47(34), 345301 (2014)
 - [43] X. B. Luo, Z. Y. Zeng, Y. Guo, B. Y. Yang, J. P. Xiao, L. Li, C. Kong, and A. X. Chen, Controlling directed atomic motion and second-order tunneling of a spin-orbit-coupled atom in optical lattices, *Phys. Rev. A* 103(4), 043315 (2021)